Enhanced high-harmonic generation from chromium-doped magnesium oxide

V. E. Nefedova*,[1] S. Fröhlich,[1] N. Tancogne-Dejean,[2] W. Boutu,[1] F. Navarrete,[3]
M. F. Ciappina,[4] D. Franz,[1] D. Gauthier,[1] A. Hamdou,[1] S. Kaassamani,[1] R. Nicolas,[1]
Q. Ripault,[1] G. Jargot,[5,6] U. Thumm,[3] M. Hanna,[5] P. Georges,[5] A. Rubio,[2] and H. Merdji†[1]

[1]*Ultrafast Nanophotonics group, LIDYL, CEA-CNRS-Université Paris-Saclay 91191, Gif-sur-Yvette, France*
[2]*Max Planck Institute for the Structure and Dynamics of Matter and Center for Free-Electron Laser Science, Luruper Chaussee 149, 22761 Hamburg, Germany*
[3]*Department of Physics, Kansas State University, Manhattan, Kansas 66506, USA*
[4]*Institute of Physics of the ASCR, ELI-Beamlines project, Na Slovance 2, 182 21 Prague, Czech Republic*
[5]*Laboratoire Charles Fabry, Institut d'Optique Graduate School, CNRS, Université Paris-Saclay, 91127 Palaiseau Cedex, France*
[6]*Fastlite, 06600 Antibes, Sophia Antipolis, France*

(Dated: March 20, 2022)

High-order harmonic generation (HHG) from crystals offers a new source of coherent extreme ultraviolet (XUV) attosecond radiation. The process is extremely sensitive to the band structure and symmetries. Here, we tailor the high-order harmonic radiation by engineering the band structure of the bulk material using dopant-induced vacancy defects. We provide a comparison of the HHG signal in the XUV domain from undoped bulk magnesium oxide (MgO) to the HHG signal from MgO doped with chromium atoms at sub-percent concentration. We experimentally demonstrate an increase in the HHG efficiency as well as an extension of the highest detectable harmonic order from chromium doped MgO with Mg vacancies below the laser-induced damage threshold. An anisotropy measurement of the harmonic emission as a function of the laser polarization shows that the crystal symmetry is preserved for the case of doped MgO. Using a reasoning based on tunneling theory, we provide an explanation about the HHG efficiency increase in MgO with dopant-induced vacancy defects. Our study paves the way towards the control of the HHG properties in solids with complex defects caused by transition metals doping. As a promising example, the energetic cutoff extension can be applied to control the attosecond emission.

I. INTRODUCTION

A. Development of efficient coherent XUV source based on HHG from solids

Since its first experimental observation[1], considerable efforts were performed in the understanding of the main mechanisms driving the high-order harmonic generation in solids (HHG). This new source of extreme ultraviolet (XUV) radiation[2,3] displays a high degree of coherence[4], for instance, suitable for lensless diffractive imaging[5]. The intrinsic essence of the solid HHG phenomenon allows the generation of ultrashort pulses controlled potentially at the sub-optical cycle of the driving laser. The nature and the properties of the HHG emission are remarkable observables of the complex attosecond electron dynamics inside the solid. Indeed, the HHG emission reflects information about the band structure of solids, providing access to intrinsic crystal properties[6,7]. The HHG process in gases can be easily explained by a single semi-classical mechanism, namely invoking what is known as the "three-step model"[8–10]. On the other hand, the interaction of the strong laser electric field with a crystal generates electron-hole pairs, which are then accelerated by this field and the resulting radiation takes its origin from an interplay of two different mechanisms[7,11–13]. One of these processes is the so-called inter-band polarization term, for which a three step model has been proposed[12], it is governed by the recombination of the electrons with the holes, leading to the emission of a burst of light of an energy equal to the instantaneous energy difference. The other mechanism is responsible for the generation of an intraband current due to the oscillations of electrons within the bands along the Brillouin zone driven by the laser field. The competition between those two mechanisms depends on the material and the driving laser parameters but, as a general feature, the intraband processes dominate the low energetic part of the HHG spectrum, while the interband contributions do in the highest energetic region and consequently the intensity of the plateau of harmonics of higher order and the cut-off. The increase of HHG yield and the extension of the highest observable harmonic in the harmonic spectrum are of high importance for the development of novel and efficient XUV sources. Various experimental techniques using solid samples as targets were already implemented to achieve those goals, such as plasmon or waveguide enhanced HHG[5,14–18]. Here, we propose an alternative way of boosting the HHG yield from solids based on doping, which paves the way towards an efficient, compact, and coherent extreme ultraviolet source. This method permits the modification and control of the material band structure for improvement of the HHG properties.

*viktoria.nefedova@cea.fr
†Corresponding author: hamed.merdji@cea.fr

B. HHG from solids with defects

Doping was demonstrated to be a considerable way to control chemical and optical properties of materials. The presence of dopants results in new electronic states in the band gap, which enable additional optical transitions[19] as well as modifications of the band gap[20–24].
Since the HHG process is very sensitive to the band structure of the materials, doping appears to be a significant leverage for influence the HHG mechanism. It is known that the tunneling rate has an exponential dependence on the band gap energy of the solid[25]. Therefore, one can expect substantial changes of the HHG yield due to modifications of the band gap. This fact has recently raised interest among theoretical works on the use of doped materials for the HHG[26–29]. For instance, the effect of impurity levels on the HHG is discussed in the theoretical investigations exploiting time-dependent density functional theory[27], where the authors have shown the enhanced HHG yield from the donor-doped material due to the electron tunneling from the impurity states to the conduction band. The reasons of the HHG signal increase can be understood by taking into account the basics of the semiconductor doping. From the one hand, donor-type dopants introduce extra electrons into the system and create states near the conduction band. From another hand, acceptor-type dopants remove electrons, thus producing unsatisfied bonds and resulting in the appearance of the holes. Impurity levels due to the presence of dopants appear within the band gap. In case of donor-type dopants, the highest occupied orbital is the impurity orbital within the band gap, while in case of acceptor-type dopands the highest occupied orbitals of the doped and undoped materials are the same.
In this work, we exploit the more complex system, in which the donor-dopants not only substitute the lattice atoms providing additional electrons but also create vacancies. Our aim is the experimental determination of changes in the HHG yield caused by the dopant-induced vacancies.

C. Chromium-doped magnesium oxide for HHG

The presence of dopant atoms in a crystal results in the emergence of impurity energy levels in the band gap[30] as well as modifications of the initial band distribution[31,32]. Another significant effect of the doping is the appearance of point defects such as vacancies and interstitial sites[33]. When a Cr dopant is introduced in the magnesium oxide (MgO) lattice, it occurs in a 3+ stable state[34–36], Cr^{3+} ions replace Mg^{2+} ions and as a consequence Mg vacancies appear to maintain charge neutrality[36]. This effect was widely studied previously and a great amount of experimental works attributed the luminescence around 700 - 800 nm to Cr^{3+} ions in different sites of the MgO lattice[19,34,37–39]. Although experimental determination of vacancies is a very challenging task, the presence of Mg vacancies in chromium-doped magnesium oxide (MgO:Cr) was also confirmed by the use of X-ray photoelectron spectroscopy technique[40]. The presence of vacancies is known to have a considerable influence on the band gap of the material[41].
In this work, we provide an experimental comparison of the HHG signals obtained in the XUV domain, generated from pristine MgO and MgO:Cr crystals. We demonstrate an enhancement of the high harmonic conversion efficiency below the damage threshold as well as an extension of the highest observable harmonic in the case of the HHG from MgO:Cr. Furthermore, we perform a comparison of the anisotropy dependence for both samples, showing that the symmetries are preserved, even if the harmonic yield is increased.
This paper is organized as follows: in the next section, Sec. II, we provide an optical characterization of the samples used in this work. Next, in the Sec. III we describe the experimental setup for the HHG. Sec. IV is focused on the obtained results. In Sec. V the experimental results are discussed. Finally, Sec. VI concludes this paper and gives an outlook on future possibilities.

II. OPTICAL CHARACTERIZATION OF PRISTINE AND CHROMIUM-DOPED MAGNESIUM OXIDE

In order to establish the possible presence of Cr^{3+} ions in our MgO:Cr sample and its subsequent influence on the band gap energy, we perform optical characterization measurements providing the difference between MgO and MgO:Cr. The measurements of photoluminescence signal from MgO and MgO:Cr (see Appendix A) used in the current work confirm the presence of Cr^{3+} ions in MgO:Cr sample, as it was introduced in Section I C. This fact is in turn associated with a consequent formation of Mg vacancies.

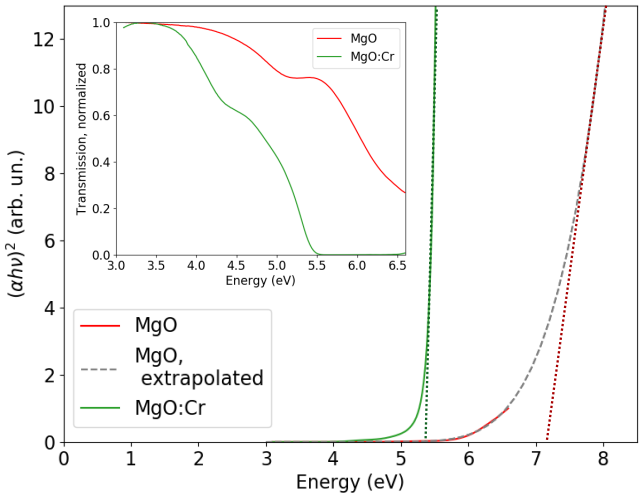

FIG. 1: Tauc plots (and transmission curves as an insert) of MgO and MgO:Cr samples, where $h\nu$ is a photon energy, α is the absorption coefficient (obtained from measured transmission data).

In order to have information about the values of the band gap energies of MgO and MgO:Cr samples with 5000 ppm chromium concentration (corresponding to ∼ 0.5% defect concentration), we measure the transmission of white light through the samples. We use the Tauc method of optical absorption edge determination[42], wherein the obtained Tauc plots are shown in Fig. 1. The linear region of the curve has to be extrapolated for a determination of the band gap energy. It can be inferred from the data that the band gap energy of MgO:Cr is about 5.36 eV. The determination on an the exact value for the MgO sample is not accessible due to limitations of spectral sensitivity of our detector. We therefore use a fifth-order polynomial extrapolation in order to estimate the band gap energy of the MgO sample, which provides the value about 7.16 eV. Thus, the obtained band gap energy difference of MgO compared to that of MgO:Cr is found to be around 1.8 eV. It should be noted, that the commonly used value of the band gap energy of the pristine MgO is 7.8 eV, *e.g.,* Ref.[43]. The observed discrepancy of the band gap energy in our work and already reported results could take origin from the minor amount of impurities, as it is detected during photoluminescence measurements (see Appendix A).
The observed modification of the band structure with the consequent band gap narrowing of MgO:Cr compared to MgO results from the presence of vacancies due to Cr^{3+} in MgO[23,24]. This fact is supported by our results on PL and transmission measurements. Since the HHG process is very sensitive to the band gap modifications, as it was introduced in Section I B, we investigate this effect in the following part of our work.

III. EXPERIMENTAL SETUP

In this work, we generate harmonics in the XUV range using an intense infra-red (IR) driving field. The experiment, sketched in Fig. 2, is carried out in vacuum, at normal incidence, using a linearly-polarised laser with a wavelength centered at $\lambda_{IR} = 1.55\,\mu$m (corresponding to a photon energy of 0.80 eV), a 125 kHz repetition rate, a pulse energy on the target of up to 4 μJ, and a pulse duration of 22 fs full width at half maximum (FWHM), more details on the laser system are provided in Appendix B. The laser beam is focused by a lens of focal length of $f = 5$ cm. The intensity at the focus is estimated based on focal length, laser pulse duration, beam size and energy. The laser intensity values provided below in the text are vacuum intensities. The maximum intensity estimated at the focus is I=22.5 TW/cm^2. The laser intensity at focus is varied by rotating the half-wave plate, and the harmonic signal is optimized by moving the samples on a motorized translation stage along the optical axis.

Two different samples are investigated: pristine MgO and Cr-doped MgO, both of them being 200-μm-thick with a (001) orientation. For MgO:Cr, the doping concentration of Cr atoms is 5000 ppm (corresponding to ∼ 0.5% defect concentration). The MgO:Cr sample is produced by a commercial company and chromium atoms are introduced in MgO crystal during tri-arc plasma growth[44,45]. The interaction of the intense laser pulse with the samples results in an emission of non-perturbative coherent high-order harmonics, which co-propagate with the driving laser. The fundamental beam and low-order harmonics are removed by an aluminium filter allowing only XUV light to pass through it. The high-order harmonics are spectrally resolved by a home-made spectrometer composed of a reflective concave diffraction grating and a back-illuminated CCD camera. We are able to detect the harmonics starting from the harmonic order 19 (15.2 eV) to the harmonic order 31 (24.8 eV).

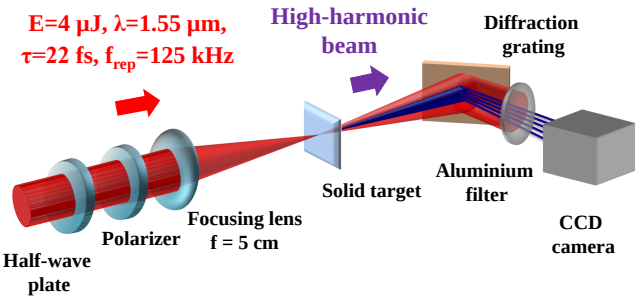

FIG. 2: (color online) Scheme of the experimental setup for HHG from MgO and MgO:Cr samples. The driving IR beam is focused into a sample producing high-order harmonics. The emitted radiation is recorded using an XUV spectrometer, which consists of a diffraction grating and a CCD camera.

IV. RESULTS

In order to investigate the possible effects of doping on the HHG, we perform identical measurements on MgO and MgO:Cr considering the variation of two main parameters: the driving laser intensity and the sample orientation with respect to laser polarisation.
We compare the strong-field response of the two samples by measuring the variation of the integrated harmonic yield generated (between 14.4 eV to 25.6 eV) as a function of the intensity of the driving field. The systematic measurements are taken under optimal conditions for each sample according to the optimization procedure described in the previous section. Our results, shown in Fig. 3 (a), demonstrate that the total high harmonic yield from MgO:Cr is stronger than from MgO up to a laser intensity of about 18 TW/cm^2. A notable feature for MgO:Cr is the presence of a plateau in between 16 TW/cm^2 and 20 TW/cm^2 while the total harmonic yield from MgO keeps increasing.
Fig. 3 (b) presents the HHG spectra obtained at the driving laser intensity of I=11.2 TW/cm^2 for MgO:Cr and at

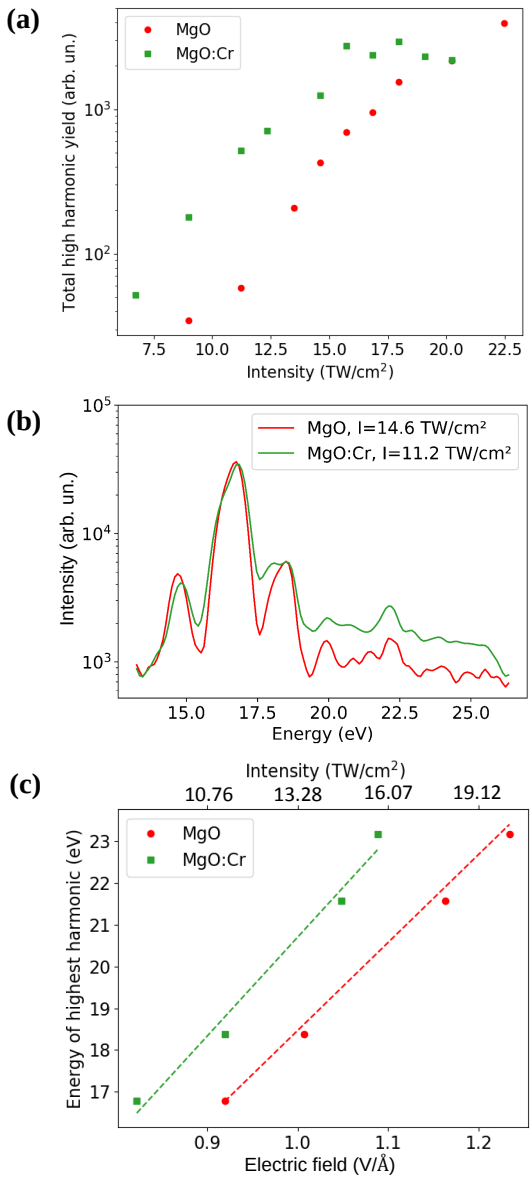

FIG. 3: HHG from pristine and doped MgO samples. Total harmonic yield as a function of driving laser intensity for MgO and MgO:Cr samples (a); HHG spectra obtained from MgO sample at a laser intensity of 14.6 TW/cm^2 and from MgO:Cr at a laser intensity of 11.2 TW/cm^2 (vacuum intensities) (b); The highest observable harmonic energy scaling with the driving field strength (c).

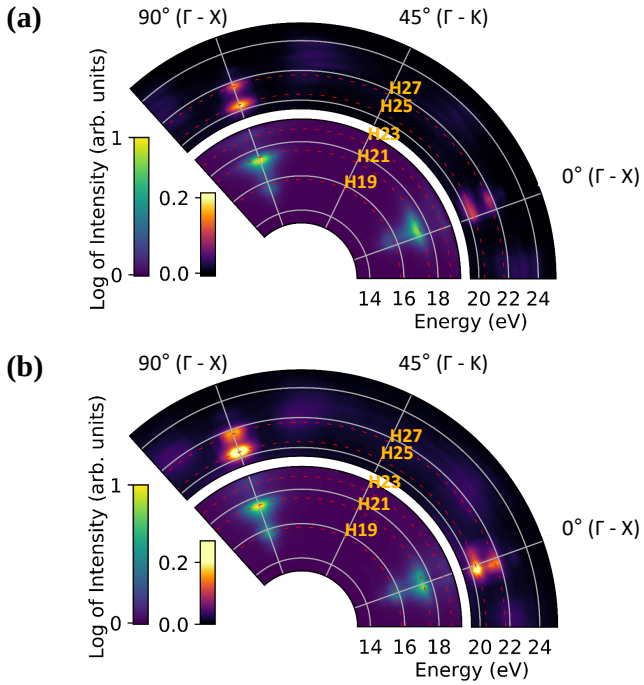

FIG. 4: Angular dependence of the harmonic spectra for MgO at a laser intensity of 20 TW/cm^2 (vacuum intensity) (a) and for MgO:Cr at a laser intensity of 15.7 TW/cm^2 (b). A four-fold symmetry is observed due to MgO cubic crystal structure. The measurements are taken with a 3 degree step.

I=14.6 TW/cm^2 for MgO. It can be inferred that the similar HHG spectra in terms of harmonic yield can be obtained using a lower driving laser intensity from MgO:Cr than from MgO.

Next, we extend our analysis comparing the scaling of the energy of the highest detectable harmonic with the driving field strength for MgO and MgO:Cr samples, which is shown in Fig. 3 (c). As can be inferred from the fitted curves, this energy scales linearly with the peak electric field strength in both cases with an almost the same slope and the energy difference between the two curves is about 2 eV for a wide range of electric-field strength. This amount of energy is in a close agreement with the band gap energy difference between MgO and MgO:Cr, as it is determined in Section II and Fig. 1.

Furthermore, we investigate the symmetries of the two samples by measuring the variation of the harmonic spectra with respect to the crystal orientation. The laser polarization is kept constant while the crystal is rotated. Fig. 4 (a, b) shows the angular dependence of the HHG spectra from MgO and MgO:Cr. The anisotropy measurements on MgO and MgO:Cr are taken at their individual optimum conditions: the optimal intensity (intensity that leads to the highest harmonic yield) for high harmonic generation from the MgO sample is 20 TW/cm^2, while it is 15.7 TW/cm^2 for MgO:Cr. As it can be seen from the obtained data, there is a clear four-fold symmetry for both, MgO and MgO:Cr samples, which is due to a cubic crystal structure of MgO. In fact, the two anisotropy maps are barely distinguishable, showing clearly that the two samples react in a very similar way and possess the same symmetries.

V. DISCUSSION

In Fig. 3(a-c) and Fig. 4(a, b) we show experimental results of the HHG spectra for both MgO and MgO:Cr, from which we can deduce that it is possible to get more energetic and intense harmonics from the sample with defects while the anisotropic behavior of the spectra (which is related to that of the sample) remains unaltered.
This striking change of behaviour induced by doping might lead to many appealing applications. Thus, a correct understanding of the underlying physics is of greatest relevance. We focus our analysis on the microscopic effects leading to the modification of the HHG spectra of the doped sample. Such an approach enables to have an access to underlying mechanisms during the HHG and has already established a direct connection to an experimental observations, *see, e.g.*, Ref.[13] and references therein. We believe that the propagation aspects play a secondary role in our case. The macroscopic effects are determined by the linear and nonlinear refractive indices, which are unlikely to exhibit large changes upon doping given the low concentration of 0.5 %[46–48].
The modification of the electron dynamics in the doped sample and its role for the HHG can be understood from a saddle point analysis[49,50] of the interband current, which has been successfully applied to the study of HHG in solids[12]. The harmonic yield derived from this approximation is proportional to[51]

$$Y \propto \exp\left[-\frac{\sqrt{8\,m_0^*}\,\varepsilon_g^{3/2}}{e\,\hbar\,E}\right] , \qquad (1)$$

where Y is the high harmonic yield, m_0^* the reduced effective mass between the highest valence and lowest conduction bands, ε_g is the minimum band gap, e is the electron charge, $\hbar$ is the reduced Planck constant and E is the laser peak electric field strength (we are using SI units here). Under this approximation, we can think of the optical process as a three step mechanism, mediated by tunneling at the center of the band. The Keldysh parameter is given by[25]:

$$\gamma = \frac{\omega_0\sqrt{\varepsilon_g\,m_0^*}}{e\,E} , \qquad (2)$$

where ω_0 is the central angular frequency of the laser. Taking into account the parameters of our experimental conditions, we find out $\gamma < 1$ (γ=0.46 for MgO and γ=0.4 for MgO:Cr), which corresponds to a tunneling regime. According to Eq. (1), one can expect the HHG yield enhancement when reducing the minimum band gap. As it was introduced in Section I C and confirmed by transmission measurements in Section II, the appearance of complex defect states due to the presence of vacancies in MgO:Cr results in band gap narrowing of approximately 1.8 eV compared to the case of MgO. Thus, this can be a reason for the increased high harmonic yield for the case of MgO:Cr compared to MgO. Considering Eq. (1) and the band gap energies E_g to be 5.36 eV for MgO:Cr and E_g to be 7.16 eV for MgO, the HHG yield is expected to be about 9 times larger from MgO:Cr compared to MgO. This fact, in turn, favors the observed increased HHG yield from MgO:Cr compared to MgO shown in Fig. 3(a).
Consequently, our analysis provides a quantitative correspondence between the experimental and theoretical amount of the HHG yield increase.

VI. CONCLUSIONS AND OUTLOOK

We perform a study aimed at the comparison of the HHG in the XUV spectral range from pristine MgO and Cr-doped MgO with vacancy defects. The obtained results demonstrate an increased HHG efficiency from MgO:Cr compared to MgO below its damage threshold as well as the extension of the highest observable harmonic in spectra at a given laser intensity. The anisotropy dependence demonstrated no change in MgO:Cr compared to MgO. The observed effect of the HHG efficiency increase from MgO:Cr compared to MgO can originate from the increased tunneling effect due to the band gap narrowing in a doped sample caused by Mg-vacancy formation in MgO lattice due to Cr in 3+ energetically favored state in Mg sites. The lower damage threshold of MgO:Cr was found to be the limiting factor for HHG using a doped sample, thus an "optimum" doping concentration can be determined which presents a compromise between efficient HHG generation on the one hand and generation below damage threshold on the other hand. Therefore, the solids doped by transition metal atoms at sub-percent doping concentration with the consequent appearance of complex vacancy defects are seen as promising candidates for the control and improvement of the HHG emission with a preserved anisotropy dependence. Our study paves the way towards the development of efficient XUV sources based on HHG in solids with defects. The attractive perspective is the future investigation of time-resolved electron dynamics in materials with dopants and complex defects.

Acknowledgments

Authors thank M. Billon for technical support. We acknowledge support from the PETACom FET Open H2020 grant number 829153, LASERLAB, support from the French ministry of research through the ANR grants 2014 IPEX, 2016 HELLIX, 2017 PACHA, the DGA RAPID grant SWIM and from the CNANO research program through the NanoscopiX grant, and the LABEX PALM (ANR-10-LABX-0039-PALM) through the grants Plasmon-X, STAMPS and HILAC. We acknowledge the financial support from the French ASTRE program through the NanoLight grant. F. N. and U. T. thank support from Air Force Office of Scientific Research under award number FA9550-17-1-0369, NSF Grant

No. 1802085 (Theory for photoemission from surfaces). M. F. C. acknowledges support by the project Advanced research using high intensity laser produced photons and particles (No. CZ.02.1.01/0.0/0.0/16 019/0000789) from European Regional Development Fund (ADONIS)

Appendix A: Photoluminescence measurements on MgO and MgO:Cr

We perform photoluminescence (PL) measurements on MgO and MgO:Cr samples and compare the obtained signals. The PL measurements are done at room temperature at 365 nm excitation. The source signal is filtered out before the detection using a long-pass filter, which transmits radiation at wavelengths longer than 514 nm. A PL signal is detected by a spectrometer (Ocean Optics).

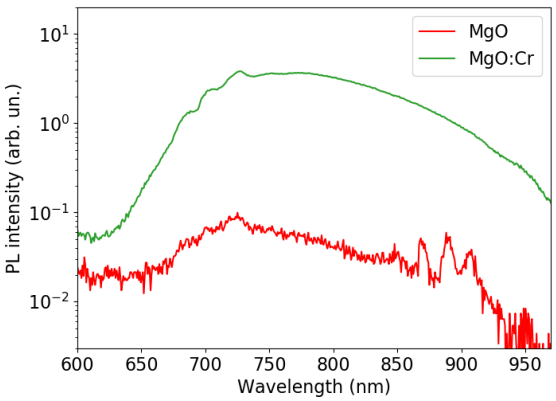

FIG. 5: Measured photoluminescence signal from MgO and MgO:Cr samples excited at 365 nm wavelength at room temperature.

Fig. 5 shows the PL signals from both samples. As can be seen, there is a strong PL signal from MgO:Cr, which consists of multiple peaks with a broad feature around 700 - 800 nm. Such a behavior of the PL signal is typically attributed to $^4T_2 \rightarrow {}^4A_2$ transitions from Cr^{3+} ions in orthorhombic sites in MgO[19,34,37]. Therefore, our PL measurements experimentally confirm the presence of Cr^{3+} ions in MgO:Cr sample, which are in turn associated with a consequent formation of Mg vacancies. This fact can be considered as the origin of the notable band gap narrowing as will be shown later.
Photoluminescence measurements in MgO reveal peaks around 720 nm as well as around 850-950 nm. We attribute these features to impurities in the undoped MgO sample, the signal around 720 nm being probably associated with Cr impurities, while multiple lines around 850-950 nm can be due to $Mg(OH)_2$ impurity phase. Similar PL behavior from MgO undoped samples was already reported in previous works[52–56].

Appendix B: OPCPA laser system

The ultrashort pulse source at 1.55 μm relies on an optical parametric chirped pulse amplifier (OPCPA) pumped by a femtosecond ytterbium-doped fiber-based laser source at 1.03 μm. This pump source delivers 400 fs, 400 μJ pulses at 125 kHz. The overall OPCPA architecture is described in details in Ref.[57]. It is seeded by a supercontinuum generation obtained from a small fraction of the pump laser in a YAG crystal. This signal is temporally stretched in a total of 5 mm of silicon, and amplified in two parametric stages. The first one is based on MgO doped periodically poled lithium niobate and the second one on KTA in non-collinear type II phase matching configuration. Compression is achieved by propagation in 210 mm of fused silica. The OPCPA output pulses are 63 fs long with an energy of 19 μJ. The pulses are then temporally compressed using soliton compression in a plate of fused silica inside a multipass cell. This results in the generation of 22 fs 14 μJ pulses at the cell output that are directed towards the HHG setup.

[1] S. Ghimire, A. D. DiChiara, E. Sistrunk, P. Agostini, L. F. DiMauro, and D. A. Reis, Nature Physics **7**, 138141 (2011).
[2] G. Vampa, C. McDonald, A. Fraser, and T. Brabec, IEEE Journal of Selected Topics in Quantum Electronics **21**, 8700110 (2015).
[3] M. Garg, M. Zhan, T. T. Luu, H. Lakhotia, T. Klostermann, A. Guggenmos, and E. Goulielmakis, Nature **538**, 359363 (2016).
[4] H. Kim, S. Han, Y. W. Kim, S. Kim, and S.-W. Kim, ACS Photonics **4**, 1627 (2017).
[5] D. Franz, S. Kaassamani, D. Gauthier, R. Nicolas, M. Kholodtsova, L. Douillard, J.-T. Gomes, L. Lavoute, D. Gaponov, N. Ducros, S. Fvrier, J. Biegert, L. Shi, M. Kovačev, W. Boutu, and H. Merdji, Scientific Reports **9**, 5663 (2019).
[6] A. A. Lanin, E. A. Stepanov, A. B. Fedotov, and A. M. Zheltikov, Optica **4**, 516 (2017).
[7] N. Tancogne-Dejean, O. D. Mücke, F. X. Kärtner, and A. Rubio, Phys. Rev. Lett. **118**, 087403 (2017).
[8] J. L. Krause, K. J. Schafer, and K. C. Kulander, Phys. Rev. Lett. **68**, 3535 (1992).
[9] P. B. Corkum, Phys. Rev. Lett. **71**, 1994 (1993).
[10] K. C. Kulander, K. J. Schafer, and K. L. Krause, Vol. 316 of NATO Advanced Study Institute Series B: Physics, Plenum, New York **68**, 95 (1993).
[11] S. Ghimire, A. D. DiChiara, E. Sistrunk, G. Ndabashimiye, U. B. Szafruga, A. Mohammad, P. Agostini, L. F. DiMauro, and D. A. Reis, Phys. Rev. A **85**, 043836 (2012).
[12] G. Vampa, C. McDonald, G. Orlando, D. Klug, P. Corkum, and T. Brabec, Phys. Rev. Lett. **113**, 073901 (2014).
[13] T. T. Luu and H. J. W orner, Phys. Rev. B **94**, 115164

(2016).
[14] S. Han, H. Kim, Y.-W. Kim, Y.-J. Kim, S. Kim, I.-Y. Park, and S.-W. Kim, Nature Communications **7**, 13105 (2016).
[15] D. Franz, B. W. Nicolas, R., L. Shi, Q. Ripault, M. Kholodtsova, B. Iwan, U. Elu Etxano, M. Kovacev, J. Biegert, and H. Merdji, "Amplification of high harmonics in 3D semiconductor waveguides", arXiv (2017).
[16] G. Vampa, B. G. Ghamsari, S. S. Mousavi, T. J. Hammond, A. Olivieri, E. Lisicka-Skrek, A. Y. Naumov, D. M. Villeneuve, A. Staudte, P. Berini, and P. B. Corkum, Nature Physics **13**, 659662 (2017).
[17] M. Sivis, M. Taucer, G. Vampa, K. Johnston, A. Staudte, A. Naumov, D. Villeneuve, C. Ropers, and P. Corkum, Science **357**, 303 (2017).
[18] K. Imasaka, T. Kaji, T. Shimura, and S. Ashihara, Optics Express **26**, 21364 (2018).
[19] B. Henderson and G. F. Imbusch, Oxford University Press **23**, 2824 (1989).
[20] D. Auvergne, J. Camassel, and H. Mathieu, Phys. Rev. B **11**, 2251 (1975).
[21] H. J. Queisser and E. E. Haller, Science **281**, 945 (1998).
[22] F. Oba and Y. Kumagai, Appl. Phys. Express **11**, 060101 (2018).
[23] C. D. Valentin and G. Pacchioni, Acc. Chem. Res. **47**, 3233 (2014).
[24] J. Robertson and S. J. Clark, Phys. Rev. B **83**, 3233 (2011).
[25] L. V. Keldysh, Sov. Phys. JETP **20**, 1307 (1965).
[26] T. Huang, X. Zhu, L. Li, X. Liu, P. Lan, and P. Lu, Phys. Rev. A **96**, 043425 (2017).
[27] C. Yu, K. K. Hansen, and L. B. Madsen, Phys. Rev. A **99**, 013435 (2019).
[28] S. de Vega, J. D. Cox, F. Sols, and F. J. G. de Abajo, ArXiv , 1910.08500v1 (2019).
[29] X.-F. Pan, T. Han, C.-L. Xia, T.-T. Xu, J. Zhang, and X.-S. Liu, Laser Phys. Lett. **16**, 115301 (2019).
[30] J. W. Lee and J.-H. Ko, Journal of Information Display **15**, 157161 (2014).
[31] T. Umebayashi, T. Yamaki, H. Itoh, and K. Asai, Appl. Phys. Lett. **81**, 454 (2002).
[32] N.Kamarulzaman, M.F.Kasim, and N.F.Chayed, Results in Physics **6**, 217 (2016).
[33] A. V. Chadwick and M. Terenzi, Springer Science & Business Media **23**, 2824 (2013).
[34] M. O. Henry, J. P. Larkin, and G. F. Imbusch, Phys. Rev. B **13**, 1893 (1976).
[35] F. Stavale, N. Nilius, and H.-J. Freund, New Journal of Physics **14**, 033006 (2012).
[36] E.Shablonin, A. I.Popov, A.Lushchik, A.Kotlov, and S.Dolgova, Physica B: Condensed Matter **477**, 133 (2015).
[37] A. Boyrivent, E. Duval, and R. Louat, Solid State Communications **19**, 1221 (1976).
[38] M. O'Neill, P.N.Gibson, and B.Henderson, Journal of Luminescence **42**, 235 (1988).
[39] T. Kato, G. Okada, and T. Yanagida, Optical Materials **54**, 134 (2016).
[40] S. Benedetti, N. Nilius, and S. Valeri, J. Phys. Chem. **119**, 25469 (2015).
[41] J. Wang, Z. Wang, B. Huang, Y. Ma, Y. Liu, X. Qin, X. Zhang, and Y. Dai, ACS Appl. Mater. Interfaces **4**, 4024 (2012).
[42] J. Tauc, R. Grigorovici, and A. Vancu, Physica Status Solidi **15**, 627 (1966).
[43] D. M. Roessler and W. C. Walker, Phys. Rev. **159**, 733 (1967).
[44] J. Czochralski, Z. Phys. Chem. **92**, 219 (1918).
[45] D. Fort, Review of Scientific Instruments **68**, 3504 (1997).
[46] A. Miller and D. Finlayson, CRC Press , 315 (1997).
[47] J. Philip, C. DAmico, G. Cheriaux, A. Couairon, B. Prade, and A. Mysyrowicz, Phys. Rev. Lett. **95**, 163901 (2005).
[48] Y. Guo, S. Lu, L. Su, C. Zhao, H. Zhang, and S. Wen, Applied Optics **54**, 953 (2015).
[49] M. Lewenstein, P. Balcou, M. Y. Ivanov, A. L'Huillier, and P. B. Corkum, Phys. Rev. A **49**, 2117 (1994).
[50] R. Wong, *Asymptotic Approximations of Integrals*, Vol. 34 (Society for Industrial and Applied Mathematics., Philadelphia, PA, USA, 2001).
[51] F. Navarrete, M. F. Ciappina, and U. Thumm, Phys. Rev. A **100**, 033405 (2019).
[52] C.-C.Chao, Journal of Physics and Chemistry of Solids **32**, 2517 (1971).
[53] Y. Kawaguchi, Solid State Communications **117**, 17 (2001).
[54] T. Kato, G. Okada, and T. Yanagida, Ceramics International **42**, 5617 (2016).
[55] W. A. Sibley, C. M. Nelson, and Y. Chen, J. Chem. Phys. **48**, 4582 (1968).
[56] C. Vaz, C. Moutafis, M. Buzzi, and J. Raabe, Journal of Electron Spectroscopy and Related Phenomena **189**, 1 (2013).
[57] G. Jargot, N. Daher, L. Lavenu, X. Delen, N. Forget, M. Hanna, and P. Georges, Opt. Lett. **43**, 5643 (2018).